Basicity of Isostructural Porous Ionic Crystals Composed of Nb/Ta-Substituted Keggin-Type Polyoxotungstates

Zhewei Weng,[a] Naoki Ogiwara,[a] Daisuke Yokogawa,[a] Takashi Kitao,[b,c] Yuji Kikukawa,[d] Sayaka Uchida*[a]

a. Department of Basic Science, School of Arts and Sciences, The University of Tokyo, 3-8-1 Komaba, Meguro-ku, Tokyo 153-8902, Japan.

b. Department of Applied Chemistry, School of Engineering, The University of Tokyo, 7-3-1 Hongo, Bunkyo-ku, Tokyo 113-8656, Japan.

c. Department of Advanced Materials Science, School of Frontier Sciences, The University of Tokyo, 5-1-5 Kashiwanoha, Kashiwa, Chiba 277-8561, Japan.

d. Department of Chemistry, Graduate School of Natural Science and Technology, Kanazawa University, Kakuma-machi, Kanazawa, Ishikawa 920-1192, Japan.

Experimental details

Experimental details

Materials

$Cr(NO_3)_3 \cdot 9H_2O$, KOH, KCl, H_3BO_3, $Na_2SiO_3 \cdot nH_2O$, $Na_2WO_4 \cdot 2H_2O$, Nb_2O_5, conc. HCl, conc. HNO_3, hydrogen peroxide, distilled water (H_2O), ethanol, acetonitrile (CH_3CN), methanol (CH_3OH), formic acid, and diethyl ether were purchased from Kanto Chemical Co. Inc. Biphenyl, malononitrile, and benzalmalononitrile were purchased from TCI Co. Ltd. Ta_2O_5 was purchased from FUJIFILM Wako Pure Chemical Corporation. All chemicals were used without further purification. $[Cr_3O(OOCH)_6(H_2O)_3](OOCH) \cdot nH_2O$,[1] $[Cr_3O(OOCH)_6(H_2O)_3](NO_3)$,[2] $K_5[BW_{12}O_{40}] \cdot nH_2O$,[3] $K_5[SiW_{11}Nb(O_2)O_{39}]$,[4] and $K_5[SiW_{11}Ta(O_2)O_{39}] \cdot 18H_2O$[5] were synthesized according to literature methods.

Characterization

Elemental analysis was performed by combustion analysis (vario MICRO cube, Elementar) for C and N, inductively coupled plasma optical emission spectrometry (ICP-OES) (ICP-OES720, Agilent Technologies) for P and W, X-ray fluorescence (XRF) analysis (EDXL300, Rigaku) for Nb and Ta, and atomic absorption spectrometry (AAS) (Hitachi, ZA3000) for K and Cr. Prior to the ICP-OES and AAS measurements, conc. HNO_3 (3 mL) was added to ca. 10 mg (accurately weighed) of the compounds to dissolve the solid completely into water (50 mL). FT-IR spectra were recorded by the KBr pellet method with a JASCO FT-IR 4100 spectrometer (JASCO) equipped with a TGS detector. Thermogravimetry-differential thermal analysis (TG-DTA) was conducted with a Thermo Plus 2 thermogravimetric analyzer (Rigaku) with α-Al_2O_3 as a reference under a dry N_2 flow (100 mL min^{-1}) in the temperature range of 298–773 K and an increasing rate of 10 K min^{-1}. Powder XRD (PXRD) patterns were measured with a D8 advance X-ray diffractometer (Bruker) by using Cu Kα radiation (λ = 1.54056 Å, 40 kV–40 mA) in the range of 3–50°. Cell parameter refinement was performed by the Pawley method.[6] H_2O, CH_3OH, and CH_3CN (298 K) sorption isotherms were measured using a volumetric gas sorption apparatus Belsorp-max (MicrotracBEL Corp.). N_2 (77 K) adsorption isotherms were measured using a volumetric gas sorption apparatus Belsorp-mini II (MicrotracBEL Corp.). Prior to the measurements, about 0.1 g of the compounds (accurately weighed) were treated under vacuum at 298 K for > 3 h to remove the water of crystallization. (Ad)sorption equilibrium was judged by the following criteria: ±0.3% of pressure changes in 500 s. Time courses of CH_3OH sorption were measured with a Thermo Plus 2 thermogravimetric analyzer (Rigaku Corporation) with α-Al_2O_3 as a reference at 303 K under a N_2 flow (30 mL min^{-1}) saturated with CH_3OH vapor. Prior to the measurements, about 10 mg of the compound was treated under a dry N_2 gas flow at 303 K to remove the water of crystallization. No significant changes were observed among the rates and equilibrium amounts of different runs. *In situ* IR spectra under CH_3OH vapor were recorded on a FT/IR-6600 (JASCO) by transmission method with a sample-coated Si disk. On one side of the Si disk (20 mmφ × 0.5 mmt), samples suspended in diethyl ether were dropped and air dried. Prior to the measurements, the Si disks were treated under vacuum for 10 min and exposed to CH_3OH vapor (10 kPa) at 298 K. Then, the pressure was reduced to 50 Pa to remove the physisorbed CH_3OH molecules. Note that the signal-to-ratio of each spectrum in Fig. 4b varied among the three samples because the background may change depending on the sample dispersion and how the Si disk is set in the IR cell holder. The absolute intensity of the *y*-axis in Fig.4b (absorbance) semi-quantitatively reflects the amount of CH_3OH sorbed on the sample.

Computational details

Electronic structure calculations were performed with the density functional theory (DFT) with CAM-B3LYP functional.[7] The employed basis sets were jun-cc-pV(D+d)Z for O, cc-pVDZ for B and Si, and SBKJC-VDZ effective core potential for Nb, Ta, and W. The geometries were taken from the crystal structures. All calculations were performed with the Gaussian16 program[8] and the natural charges were computed using the NBO 7.0 program.[9]

Table S1 Crystallographic data of **1_POM**

Compound	**1_BW$_{12}$**	**1_SiW$_{11}$Nb**	**1_SiW$_{11}$Ta**
Empirical formula	$C_6H_{38}BK_4Cr_3W_{12}O_{69}$	$C_6H_{34}SiK_4Cr_3NbW_{11}O_{67}$	$C_6H_{38}SiK_4Cr_3TaW_{11}O_{69}$
Formula weight	3743.60	3633.91	3757.98
Temperature (K)	153	153	153
Wavelength (Å)	0.71073	0.71073	0.71073
Crystal system	Orthorhombic	Orthorhombic	Orthorhombic
Space group	*Pnma*	*Pnma*	*Pnma*
a (Å)	24.3679(4)	24.4216(4)	24.4565(4)
b (Å)	15.9691(2)	16.0494(2)	16.0527(4)
c (Å)	16.9507(2)	17.0259(2)	17.0555(4)
α (°)	90	90	90
β (°)	90	90	90
γ (°)	90	90	90
Volume (Å^3)	6596.11(16)	6673.31(17)	6695.9(3)
Z	4	4	4
F(000)	6444	6348	6476
θ range (°)	4.844 to 60.864	4.784 to 60.962	4.776 to 60.908
Reflections collected	39997	44291	41684
GoF on F^2	1.175	1.055	1.069
R_1[a] [$I > 2\sigma(I)$]	0.0637	0.0658	0.1052
wR_2[b] [$I > 2\sigma(I)$]	0.1684	0.1732	0.2644

[a] $R_1 = \sum||F_o|-|F_c||/\sum|F_o|$; [b] $wR_2 = [\sum w(F_o^2-F_c^2)^2/\sum w(F_o^2)^2]^{1/2}$.

Table S2 Catalytic results in Knoevenagel condensation reaction[a]

Entry	Catalysts	Conversion / %	Yield[b] / %	Selectivity[c] / %
1[d]	**Cr-H + $SiW_{11}Ta$**	49	32	65
2[d]	**Cr-H + $SiW_{11}Nb$**	29	18	51
3[d]	**Cr-H + BW_{12}**	16	12	73
4	**1_$SiW_{11}Ta$** (2^{nd} run)	35	22	63
5	**1_$SiW_{11}Nb$** (2^{nd} run)	29	16	55
6	**1_BW_{12}** (2^{nd} run)	19	11	57
7	**1_$SiW_{11}Ta$** (3^{rd} run)	40	25	63
8	**1_$SiW_{11}Nb$** (3^{rd} run)	32	21	65
9	**1_BW_{12}** (3^{rd} run)	22	10	43

[a]Reaction conditions: 0.01 mmol catalyst, 1.0 mmol benzaldehyde, 1.0 mmol malononitrile, 10 mg biphenyl, 1 mL CH_3CN, 353 K. [b]Yield of benzalmalononitrile. [c]Selectivity to benzalmalononitrile. [d]Partial dissolution of catalysts was observed during the reaction.

Table S3 Natural population analysis of **1_BW$_{12}$**

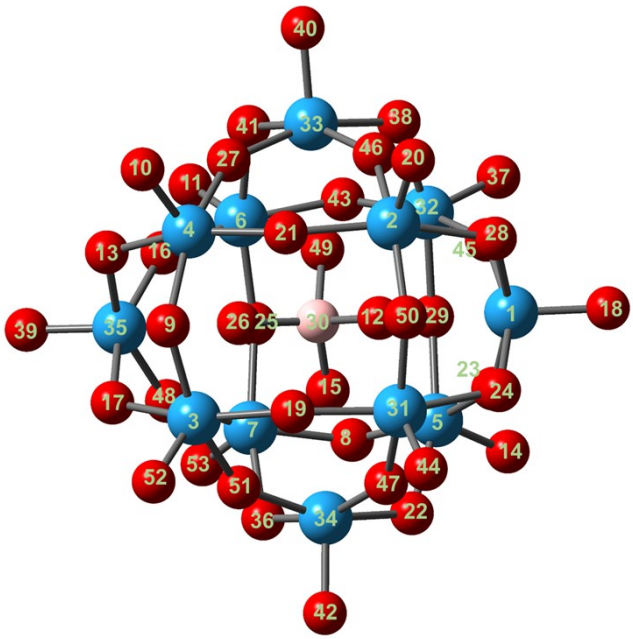

Atomic Number	Natural Charge	Atomic Number	Natural Charge
W1	2.16758	O28	–0.83136
W2	2.17225	O29	–0.83382
W3	2.1643	B30	1.48173
W4	2.16093	W31	2.16758
W5	2.16787	W32	2.1643
W6	2.18454	W33	2.16093
W7	2.17287	W34	2.16788
O8	–0.83449	W35	2.18454
O9	–0.83106	O36	–0.83449
O10	–0.6724	O37	–0.66499
O11	–0.67293	O38	–0.83106
O12	–1.14089	O39	–0.6724
O13	–0.8378	O40	–0.67293
O14	–0.65843	O41	–0.8378
O15	–1.147	O42	–0.65843
O16	–0.82315	O43	–0.83064
O17	–0.83064	O44	–0.65738
O18	–0.65738	O45	–0.83618
O19	–0.83618	O46	–0.82495
O20	–0.65725	O47	–0.83465
O21	–0.82495	O48	–0.8344
O22	–0.83589	O49	–1.13899
O23	–0.83465	O50	–0.83136
O24	–0.84254	O51	–0.83382
O25	–0.8344	O52	–0.66499
O26	–1.13899	O53	–0.65965
O27	–0.82197		

Table S4 Natural population analysis of **1_SiW$_{11}$Nb**

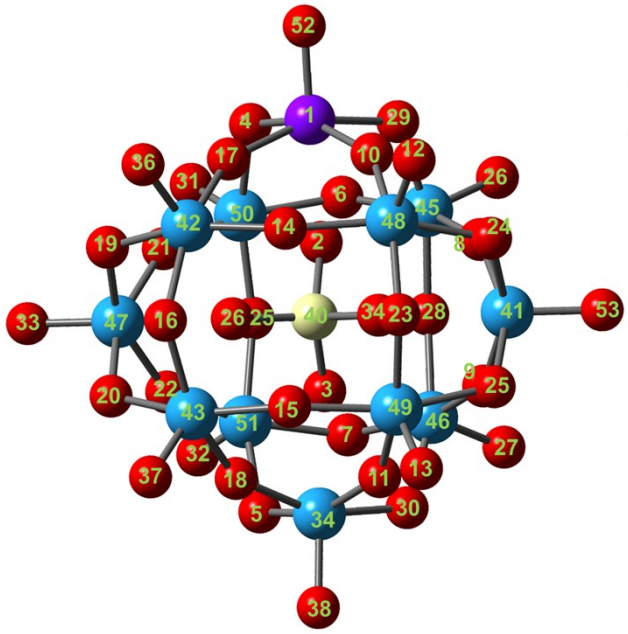

Atomic Number	Natural Charge	Atomic Number	Natural Charge
Nb1	2.09449	O28	–0.85481
O2	–1.28671	O29	–0.86014
O3	–1.27594	O30	–0.84092
O4	–0.86907	O31	–0.66765
O5	–0.83863	O32	–0.65381
O6	–0.84427	O33	–0.67892
O7	–0.84415	O34	–1.27837
O8	–0.83686	O35	–1.27324
O9	–0.84897	O36	–0.66261
O10	–0.8811	O37	–0.65613
O11	–0.85162	O38	–0.65832
O12	–0.64968	O39	–0.84196
O13	–0.64257	Si40	2.60442
O14	–0.85167	W41	2.17337
O15	–0.84503	W42	2.16578
O16	–0.85718	W43	2.17761
O17	–0.87551	W44	2.17708
O18	–0.84543	W45	2.1579
O19	–0.8365	W46	2.17002
O20	–0.84326	W47	2.17203
O21	–0.83872	W48	2.1633
O22	–0.84813	W49	2.1738
O23	–0.86381	W50	2.17913
O24	–0.84149	W51	2.18878
O25	–0.8452	O52	–0.82135
O26	–0.67611	O53	–0.65059
O27	–0.6613		

Table S5 Natural population analysis of **1_SiW$_{11}$Ta**

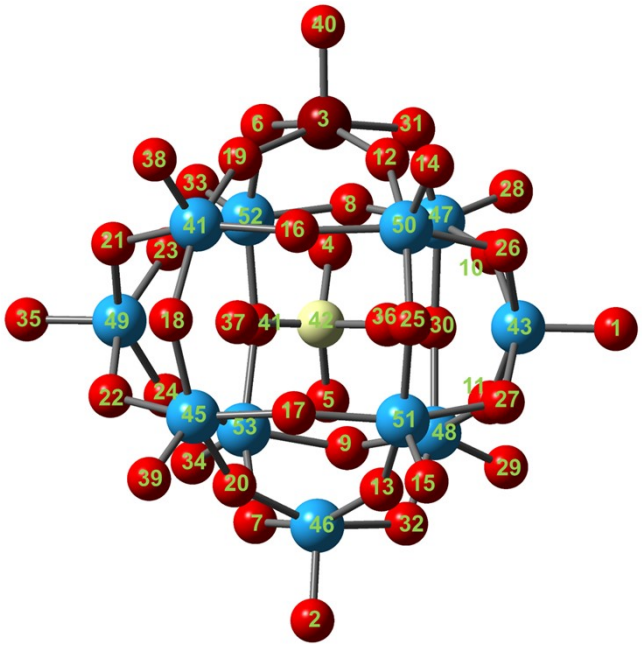

Atomic Number	Natural Charge	Atomic Number	Natural Charge
O1	–0.65605	O28	–0.67423
O2	–0.65204	O29	–0.66062
Ta3	2.14444	O30	–0.85485
O4	–1.27746	O31	–0.86495
O5	–1.27668	O32	–0.8416
O6	–0.87799	O33	–0.66629
O7	–0.83942	O34	–0.65347
O8	–0.84516	O35	–0.67841
O9	–0.84403	O36	–1.27819
O10	–0.83646	O37	–1.27356
O11	–0.84822	O38	–0.66054
O12	–0.88673	O39	–0.65599
O13	–0.85248	O40	–0.88194
O14	–0.64758	O41	–0.84229
O15	–0.64222	Si42	2.60484
O16	–0.85216	W43	2.17314
O17	–0.84505	W44	2.16959
O18	–0.85694	W45	2.17765
O19	–0.88118	W46	2.1775
O20	–0.84624	W47	2.1629
O21	–0.83624	W48	2.16992
O22	–0.84321	W49	2.17215
O23	–0.83909	W50	2.1669
O24	–0.84822	W51	2.17372
O25	–0.86355	W52	2.18441
O26	–0.84028	W53	2.18873
O27	–0.84429		

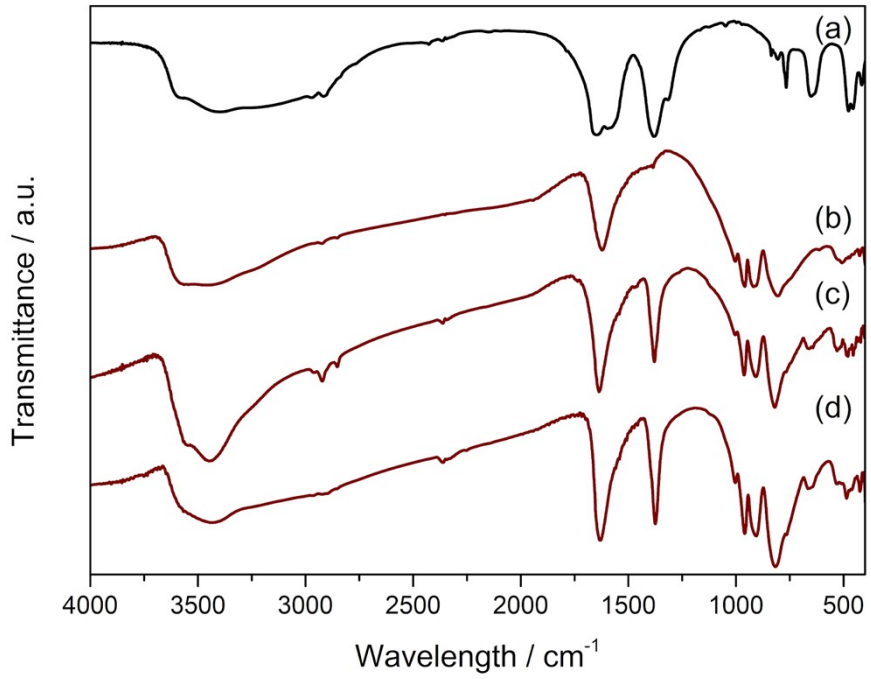

Fig. S1 IR spectra of (a) $[Cr_3O(OOCH)_6(H_2O)_3](OOCH)\cdot nH_2O$, (b) $K_5[BW_{12}O_{40}]\cdot nH_2O$, (c) **1_BW$_{12}$**, and (d) **1_BW$_{12}$** after reaction.

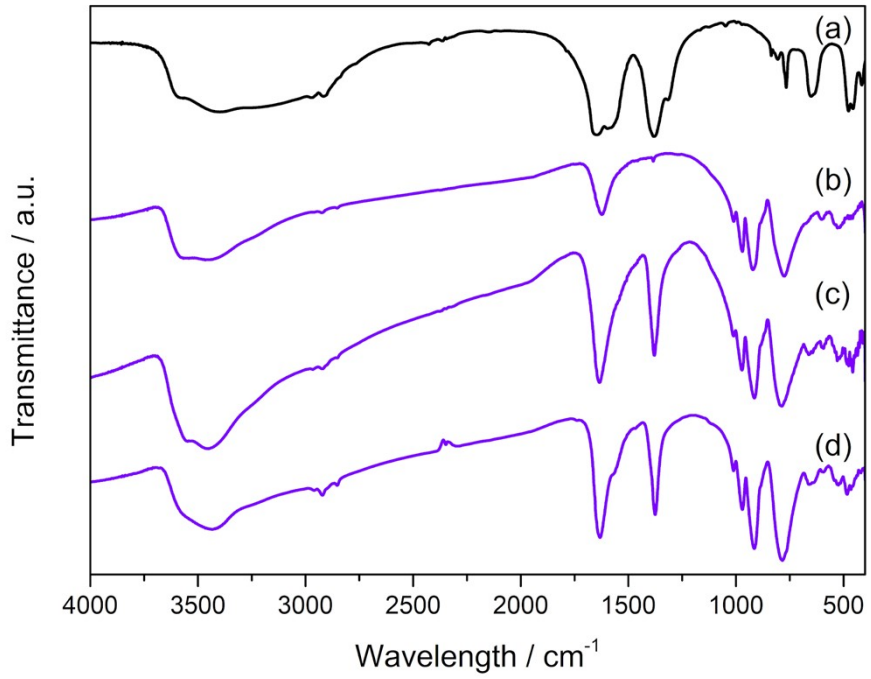

Fig. S2 IR spectra of (a) $[Cr_3O(OOCH)_6(H_2O)_3](OOCH)\cdot nH_2O$, (b) $K_5[SiW_{11}Nb(O_2)O_{39}]$, (c) **1_SiW$_{11}$Nb**, and (d) **1_SiW$_{11}$Nb** after reaction.

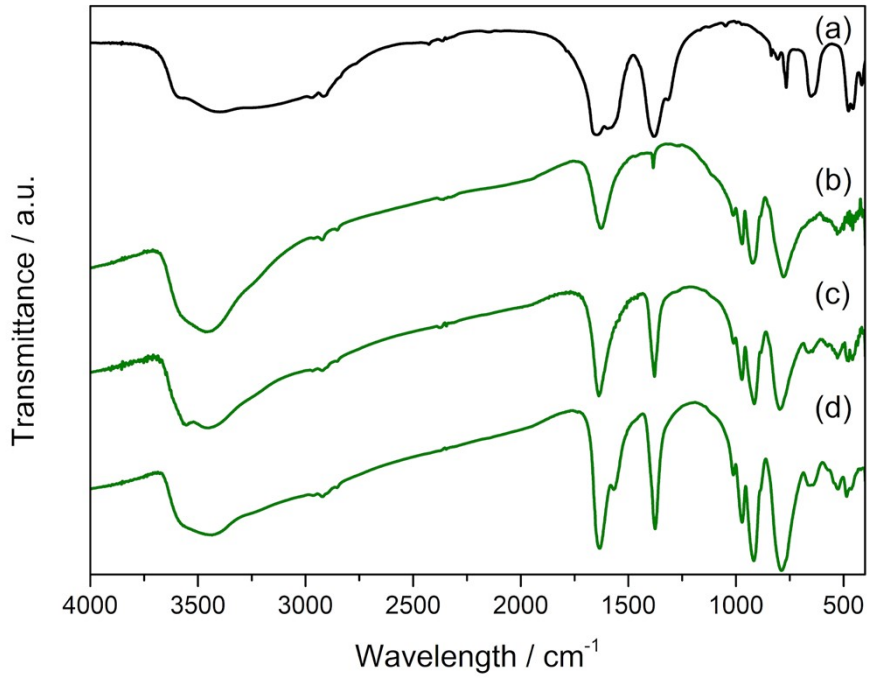

Fig. S3 IR spectra of (a) $[Cr_3O(OOCH)_6(H_2O)_3](OOCH)\cdot nH_2O$, (b) $K_5[SiW_{11}Ta(O_2)O_{39}]\cdot 18H_2O$, (c) **1_SiW$_{11}$Ta**, and (d) **1_SiW$_{11}$Ta** after reaction.

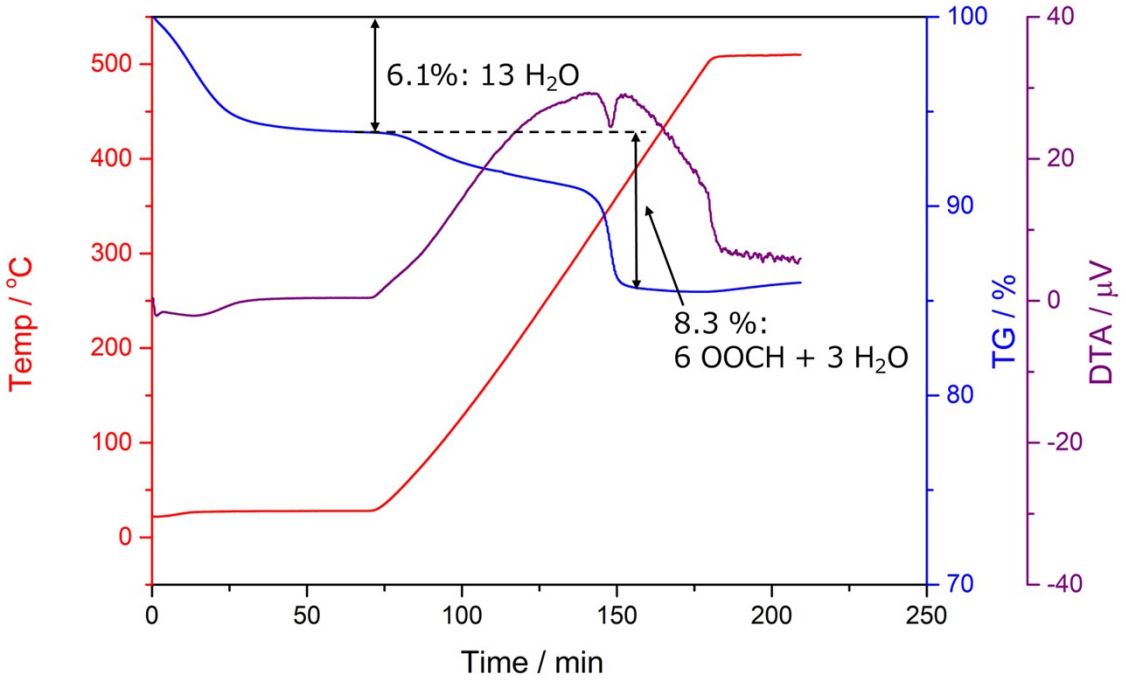

Fig. S4 TG-DTA analysis of **1_BW$_{12}$**.

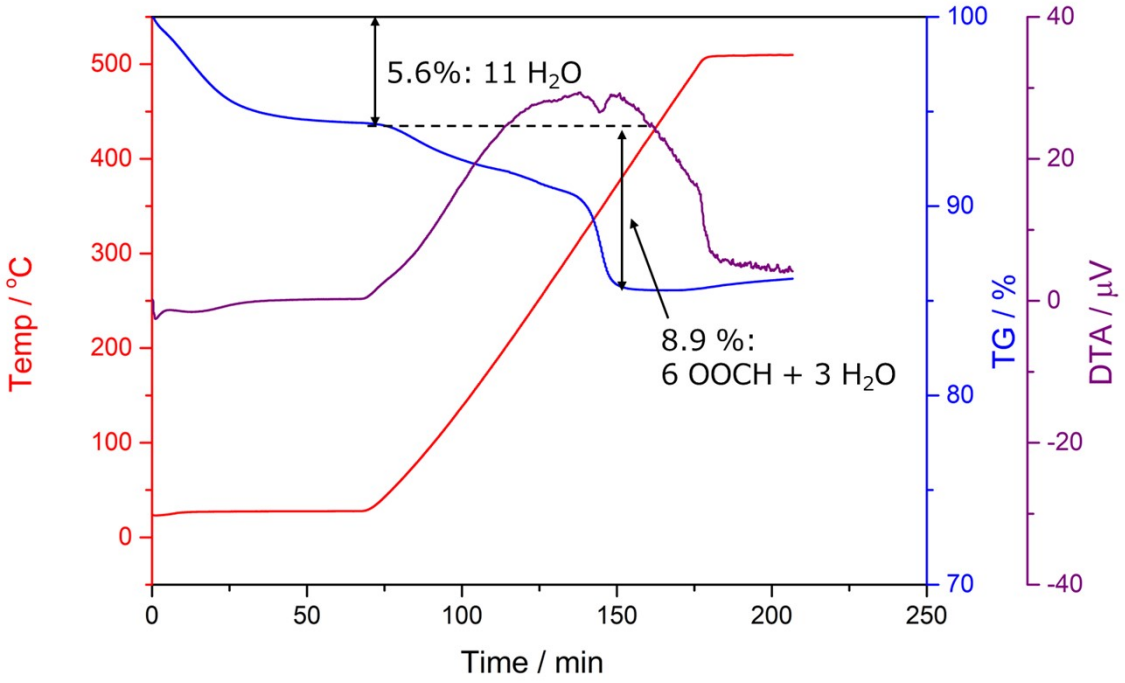

Fig. S5 TG-DTA analysis of **1_$SiW_{11}Nb$**.

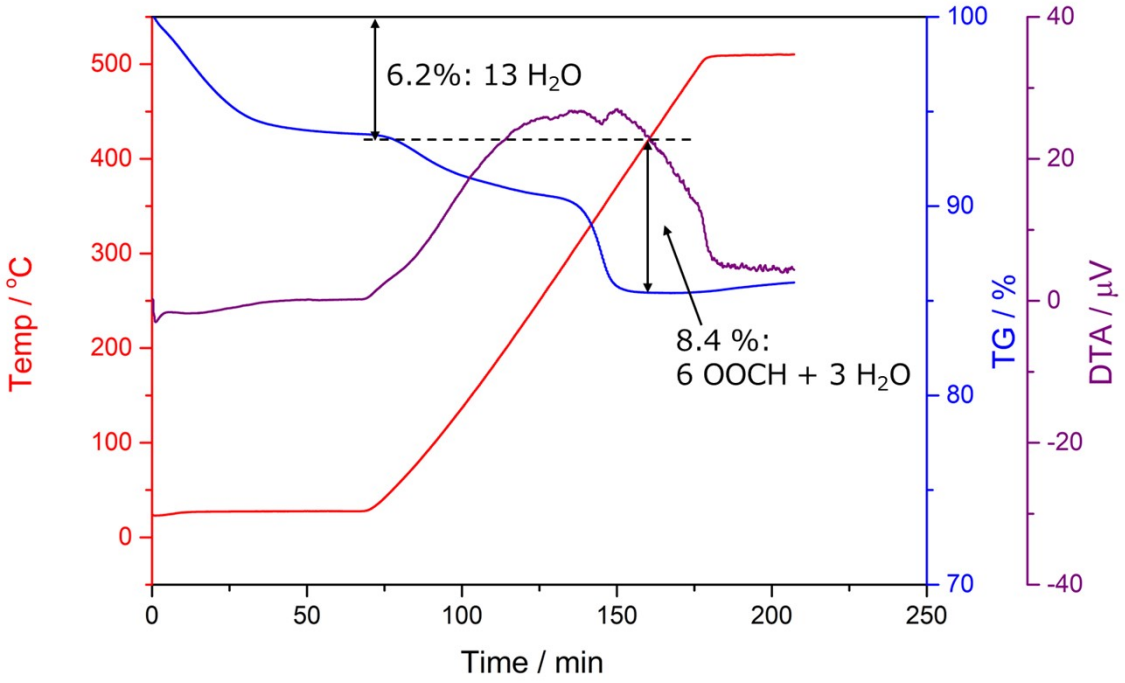

Fig. S6 TG-DTA analysis of **1_$SiW_{11}Ta$**.

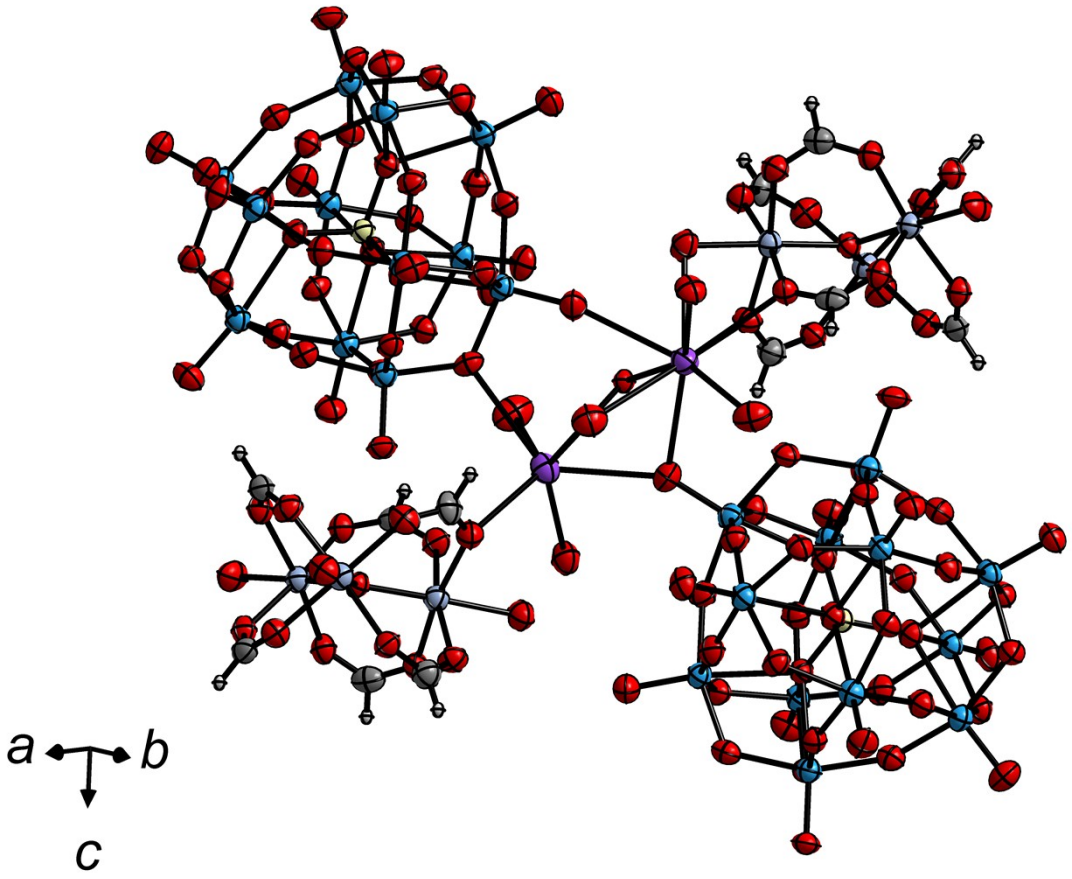

Fig. S7 ORTEP drawing of **1_BW$_{12}$** showing thermal ellipsoids at the 50% probability level. Color codes: W: blue; B: pink; O: red; Cr: violet; K: purple; C: grey; H: light grey.

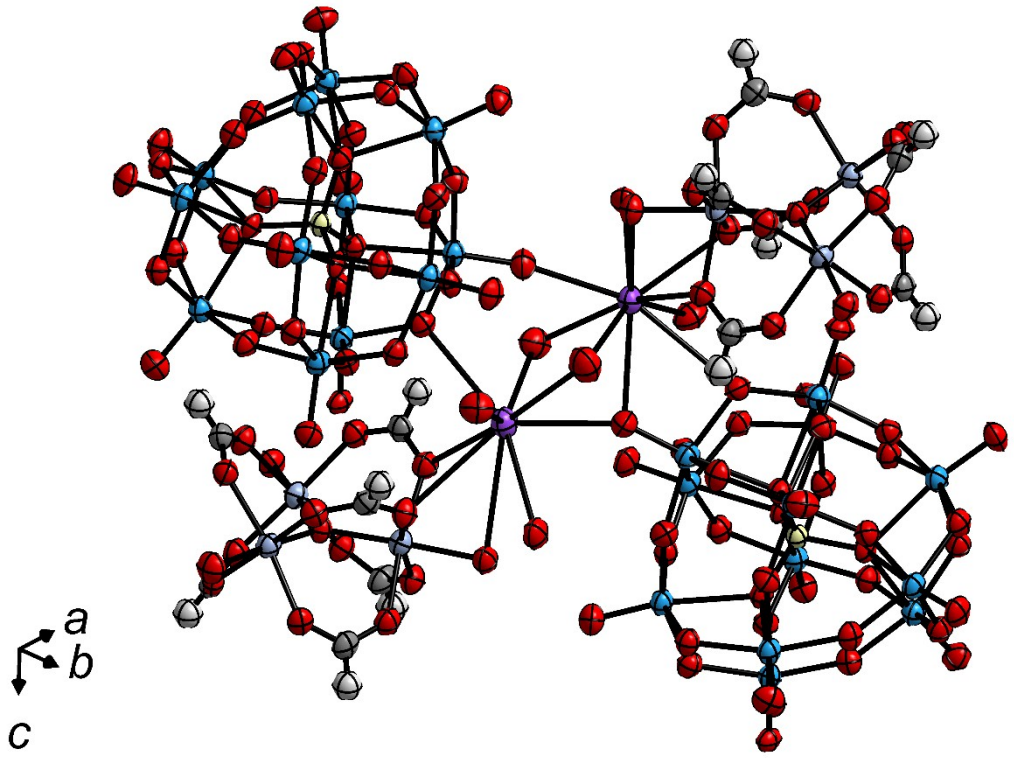

Fig. S8 ORTEP drawing of **1_SiW$_{11}$Ta** showing thermal ellipsoids at the 50% probability level. Color codes: W/Ta: blue; Si: light green; O: red; Cr: violet; K: purple; C: grey; H: light grey.

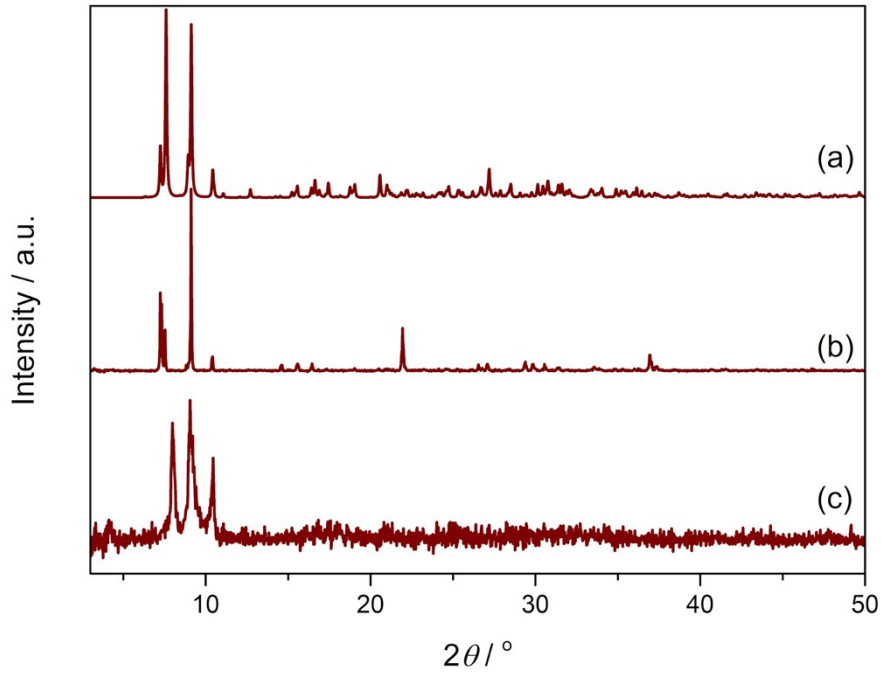

Fig. S9 PXRD patterns of **1_BW$_{12}$**. (a) Calculated, (b) experimental, and (c) after catalytic reaction.

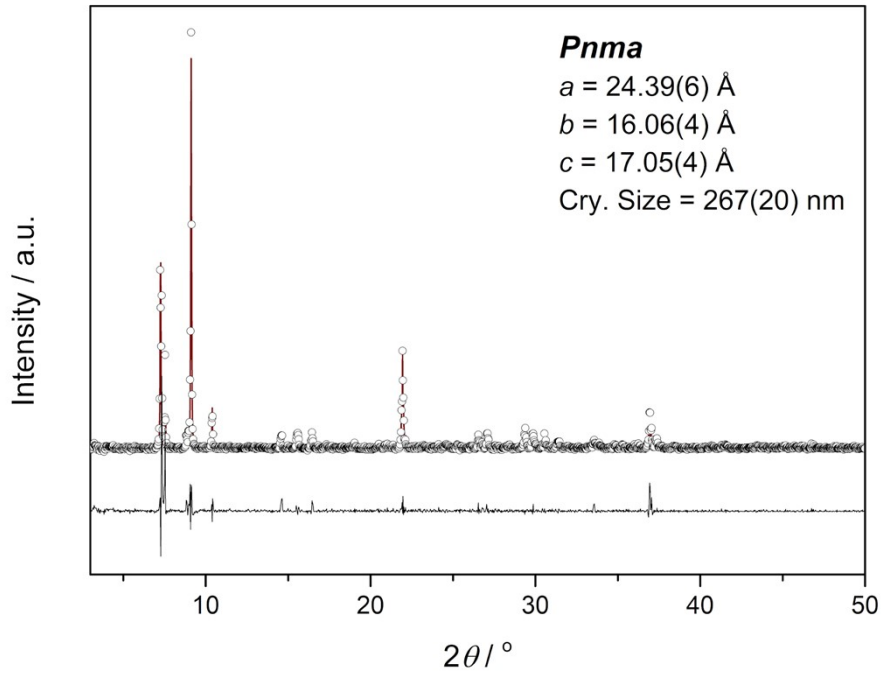

Fig. S10 Experimental (open circles) and calculated (solid line) PXRD patterns of as-synthesized **1_BW$_{12}$** by the Pawley method. The difference between the experimental and calculated data was shown under the patterns.

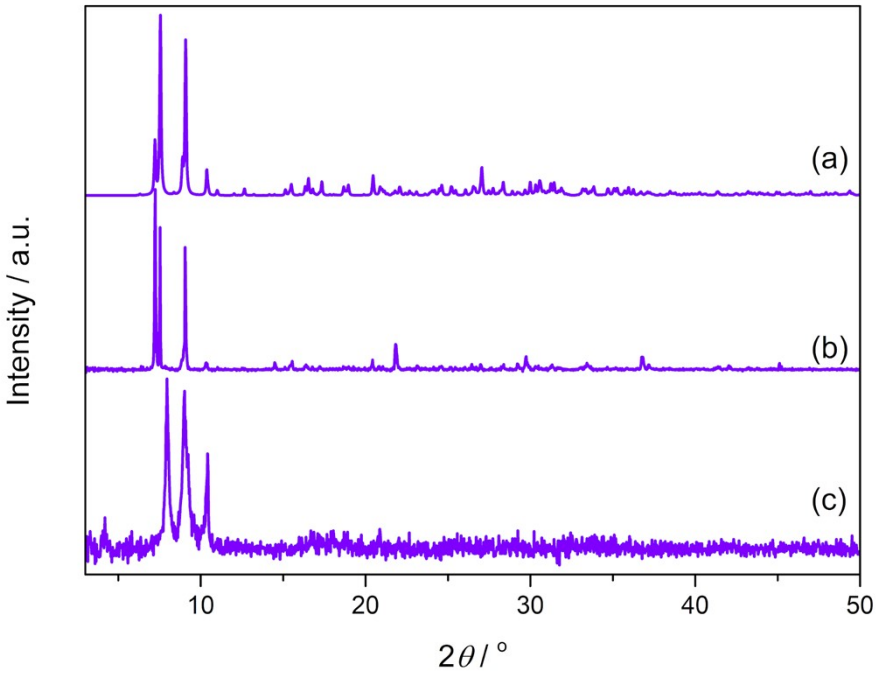

Fig. S11 PXRD patterns of **1_SiW$_{11}$Nb**. (a) Calculated, (b) experimental, and (c) after catalytic reaction.

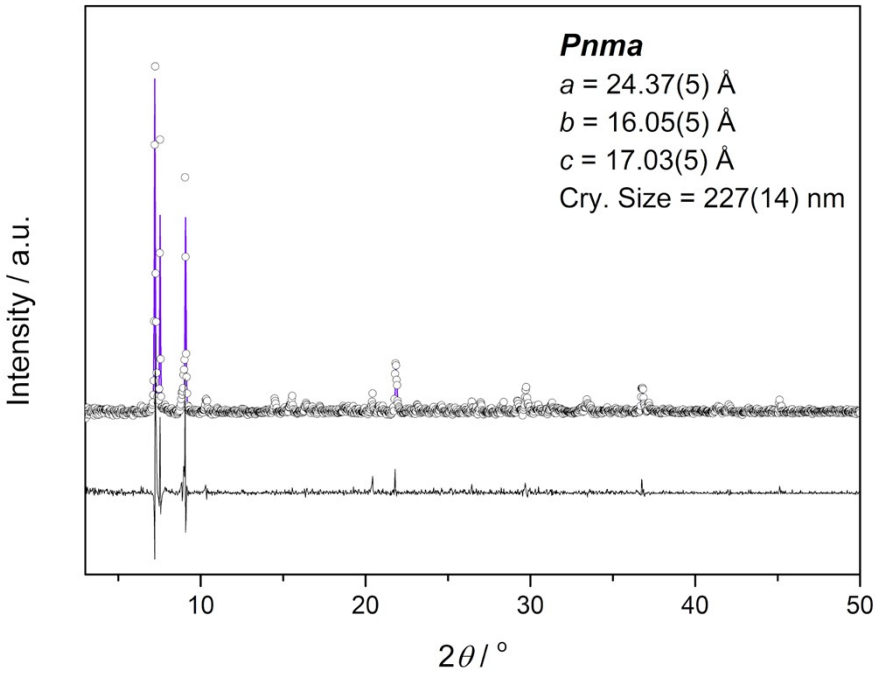

Fig. S12 Experimental (open circles) and calculated (solid line) PXRD patterns of as-synthesized **1_SiW$_{11}$Nb** by the Pawley method. The difference between the experimental and calculated data was shown under the patterns.

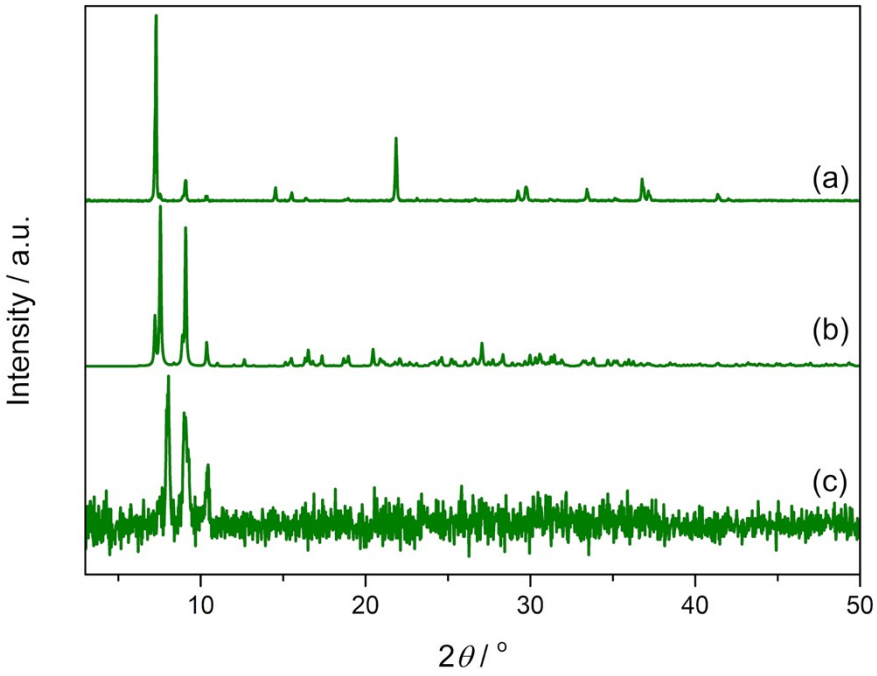

Fig. S13 PXRD patterns of **1_SiW$_{11}$Ta**. (a) Calculated, (b) experimental, and (c) after catalytic reaction.

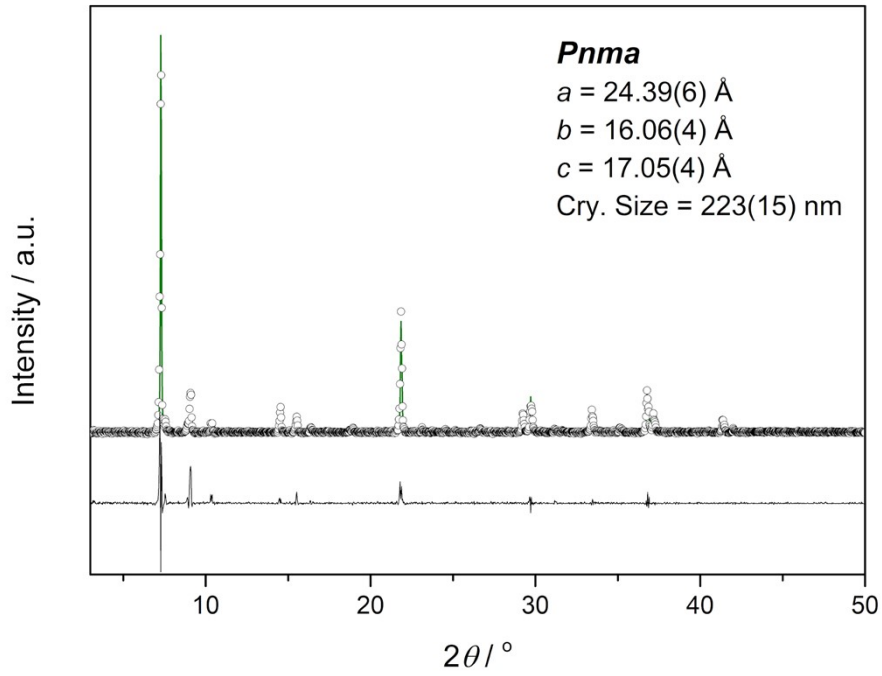

Fig. S14 Experimental (open circles) and calculated (solid line) PXRD patterns of as-synthesized **1_SiW$_{11}$Ta** by the Pawley method. The difference between the experimental and calculated data was shown under the patterns.

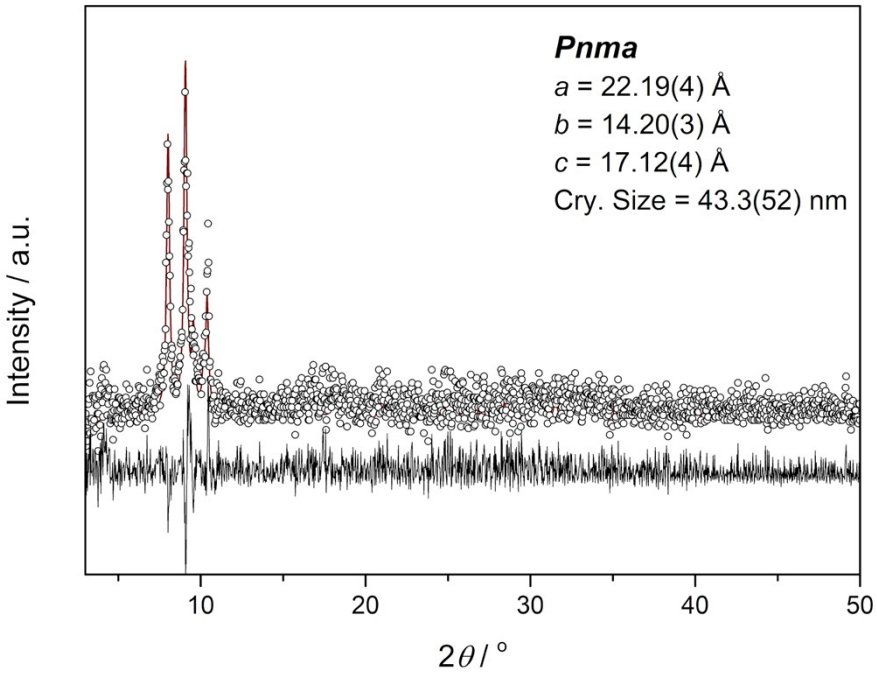

Fig. S15 Experimental (open circles) and calculated (solid line) PXRD patterns of **1_BW$_{12}$** after catalytic reaction by the Pawley method. The difference between the experimental and calculated data was shown under the patterns.

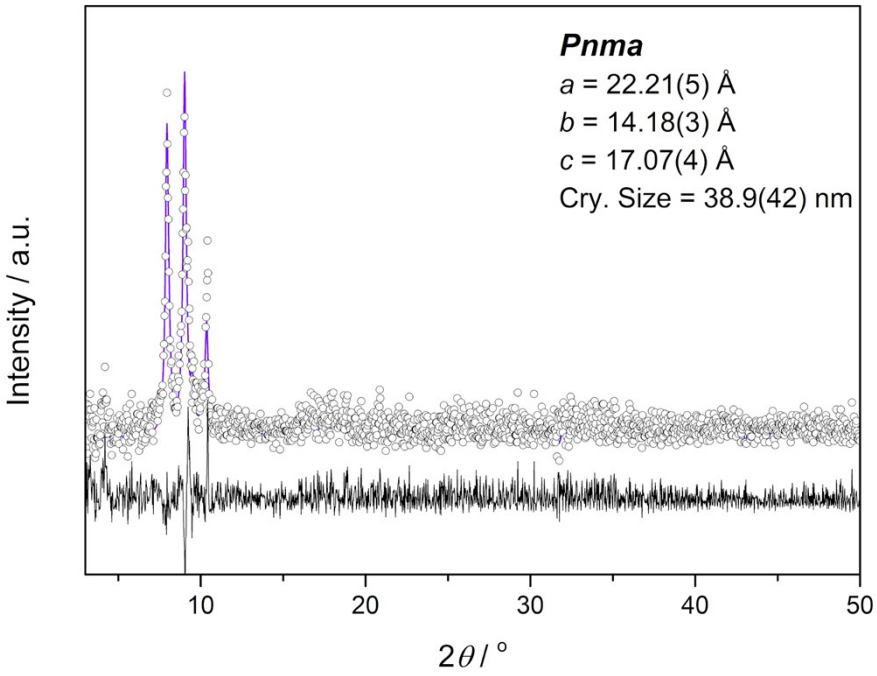

Fig. S16 Experimental (open circles) and calculated (solid line) PXRD patterns of **1_SiW$_{11}$Nb** after catalytic reaction by the Pawley method. The difference between the experimental and calculated data was shown under the patterns.

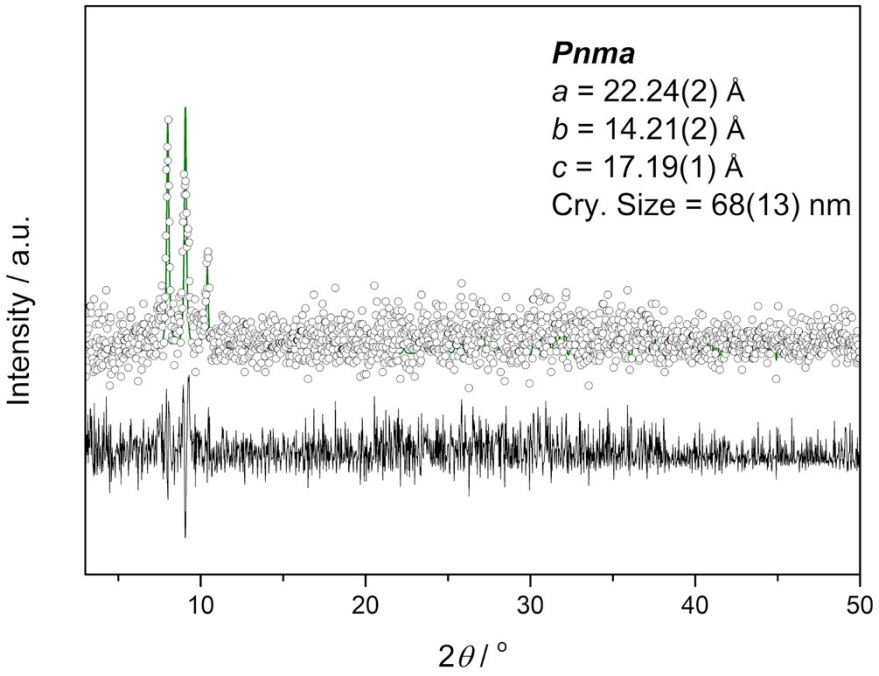

Fig. S17 Experimental (open circles) and calculated (solid line) PXRD patterns of **1_SiW$_{11}$Ta** after catalytic reaction by the Pawley method. The difference between the experimental and calculated data was shown under the patterns.

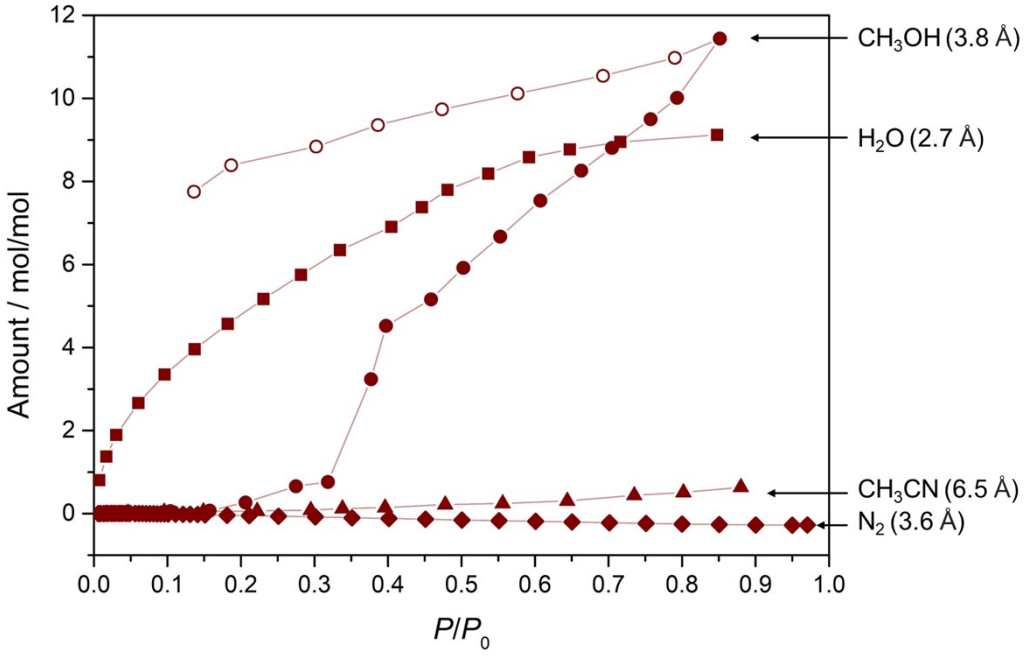

Fig. S18 H_2O (square, 298 K), CH_3OH (circle, 298 K), CH_3CN (triangle, 298 K), and N_2 (diamond, 77 K) sorption isotherms of **1_BW$_{12}$**. Solid and open symbols indicate the sorption and desorption branches, respectively. The P_0 values are 3.169 kPa,[10] 16.958 kPa,[11] and 12.186 kPa[12] for H_2O, CH_3OH, and CH_3CN, respectively, and actually measured for N_2.

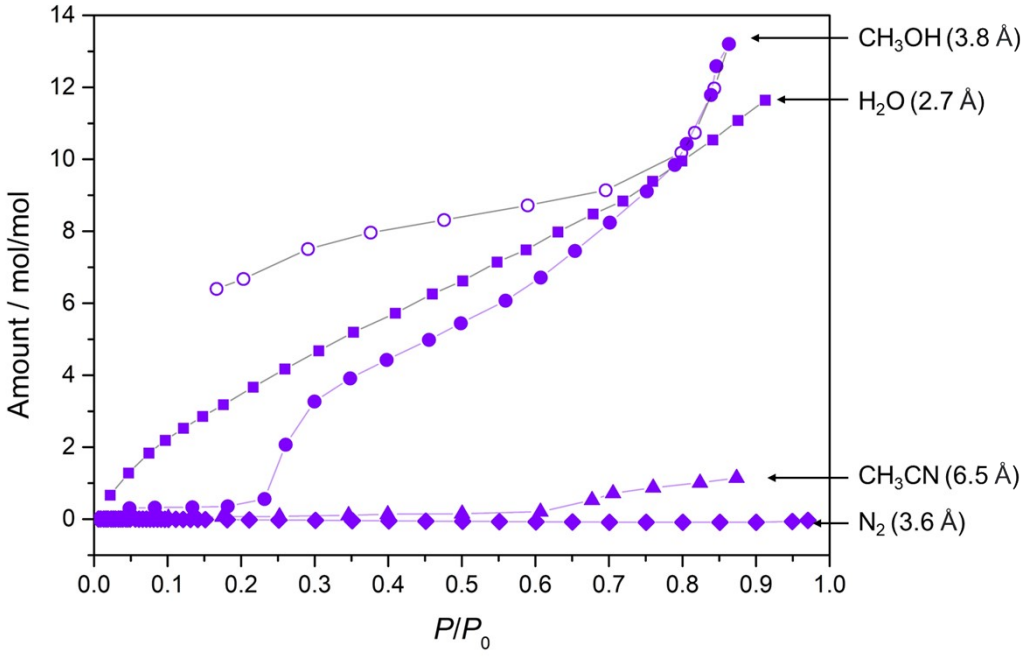

Fig. S19 H_2O (square, 298 K), CH_3OH (circle, 298 K), CH_3CN (triangle, 298 K), and N_2 (diamond, 77 K) sorption isotherms of **1_SiW$_{11}$Nb**. Solid and open symbols indicate the sorption and desorption branches, respectively. The P_0 values are 3.169 kPa,[10] 16.958 kPa,[11] and 12.186 kPa[12] for H_2O, CH_3OH, and CH_3CN, respectively, and actually measured for N_2.

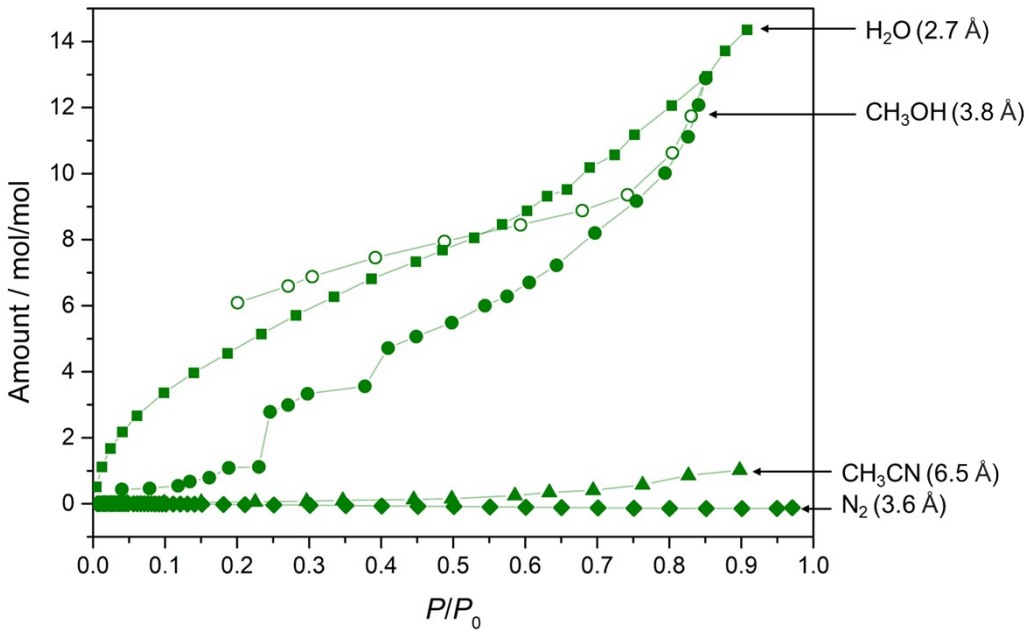

Fig. S20 H_2O (square, 298 K), CH_3OH (circle, 298 K), CH_3CN (triangle, 298 K), and N_2 (diamond, 77 K) sorption isotherms of **1_SiW$_{11}$Ta**. Solid and open symbols indicate the sorption and desorption branches, respectively. The P_0 values are 3.169 kPa,[10] 16.958 kPa,[11] and 12.186 kPa[12] for H_2O, CH_3OH, and MeCN, respectively, and actually measured for N_2.

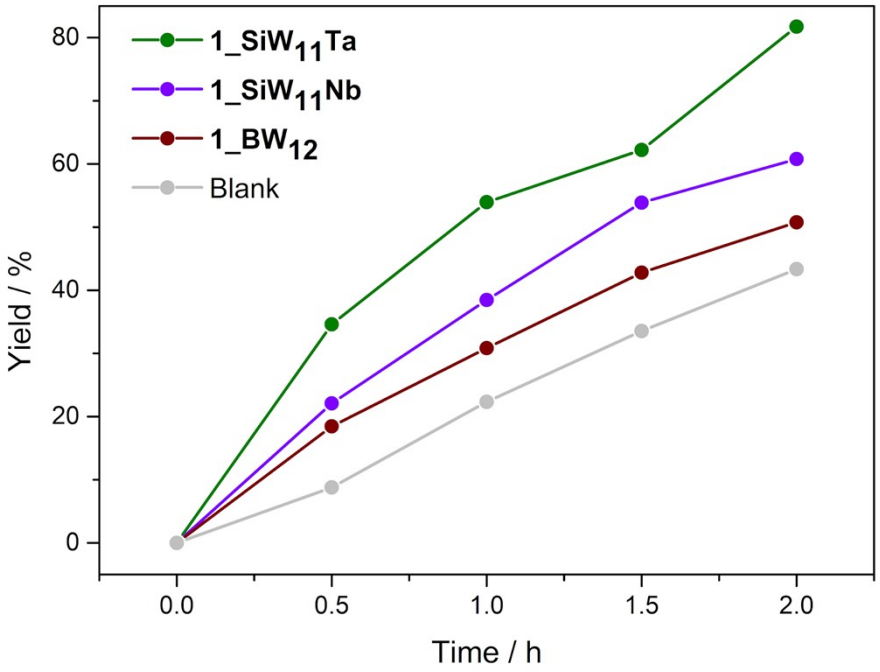

Fig. S21 Time courses of Knoevenagel condensation catalyzed by **1_SiW$_{11}$Ta** (green), **1_SiW$_{11}$Nb** (purple), **1_BW$_{12}$** (brown), and blank test (gray) at 298 K. Reaction conditions: 0.01 mmol catalyst, 1.0 mmol benzaldehyde, 1.0 mmol malononitrile, 10 mg biphenyl, and 3 mL ethanol.

Reference

1. M. K. Johnson, D. B. Powell and R. D. Cannon, *Spectrochim. Acta*, 1981, **37**, 995–1006.
2. T. Fujihara, J. Aonahata, S. Kumakura, A. Nagasawa, K. Murakami and T. Ito, *Inorg. Chem.*, 1998, **37**, 3779–3784.
3. C. Rocchiccioli-Deltcheff, M. Fournier, R. Franck and R. Thouvenot, *Inorg. Chem.*, 1983, **22**, 207–216.
4. G.-S. Kim, D. A. Judd, C. L. Hill and R. F. Schinazi, *J. Med. Chem.*, 1994, **37**, 816–820.
5. S. Shi, Y. Chen, J. Gong, Z. Dai and L. Qu, *Transition Met. Chem.*, 2005, **30**, 136–140.
6. G. S. Pawley, *J. Appl. Crystallogr.*, 1981, **14**, 357–361.
7. T. Yanai, D. Tew and N. Handy, *Chem. Phys. Lett*., 2004, **393**, 51–57.
8. Gaussian 16, Revision C.01, M. J. Frisch, G. W. Trucks, H. B. Schlegel, G. E. Scuseria, M. A. Robb, J. R. Cheeseman, G. Scalmani, V. Barone, G. A. Petersson, H. Nakatsuji, X. Li, M. Caricato, A. V. Marenich, J. Bloino, B. G. Janesko, R. Gomperts, B. Mennucci, H. P. Hratchian, J. V. Ortiz, A. F. Izmaylov, J. L. Sonnenberg, D. Williams-Young, F. Ding, F. Lipparini, F. Egidi, J. Goings, B. Peng, A. Petrone, T. Henderson, D. Ranasinghe, V. G. Zakrzewski, J. Gao, N. Rega, G. Zheng, W. Liang, M. Hada, M. Ehara, K. Toyota, R. Fukuda, J. Hasegawa, M. Ishida, T. Nakajima, Y. Honda, O. Kitao, H. Nakai, T. Vreven, K. Throssell, J. A. Montgomery, Jr., J. E. Peralta, F. Ogliaro, M. J. Bearpark, J. J. Heyd, E. N. Brothers, K. N. Kudin, V. N. Staroverov, T. A. Keith, R. Kobayashi, J. Normand, K. Raghavachari, A. P. Rendell, J. C. Burant, S. S. Iyengar, J. Tomasi, M. Cossi, J. M. Millam, M. Klene, C. Adamo, R. Cammi, J. W. Ochterski, R. L. Martin, K. Morokuma, O. Farkas, J. B. Foresman and D. J. Fox, Gaussian, Inc., Wallingford CT, 2016.
9. NBO 7.0. E. D. Glendening, J. K. Badenhoop, A. E. Reed, J. E. Carpenter, J. A. Bohmann, C. M. Morales, P. Karafiloglou, C. R. Landis and F. Weinhold, Theoretical Chemistry Institute, University of Wisconsin, Madison WI, 2018.
10. D. R. Lide, *CRC Handbook of Chemistry and Physics, 85th Edition*, CRC Press, 2004.
11. H. F. Gibbard and J. L. Creek, *J. Chem. Eng. Data*, 1974, **19**, 308–310.
12. G. Heim, *Bull. Soc. Chim. Belg.*, 1933, **42**, 467–482.